This is a repository copy of *Directional Transportation of Impacting Droplets on Wettability-Controlled Surfaces*.

Version: Accepted Version

Article:

Directional transportation of impacting droplets on wettability-controlled surfaces

Fuqiang Chu,[1,2†] *Jia Luo,[2,3‡]* *Chonglei Hao,[4]* *Jun Zhang,[2]* *Xiaomin Wu,[5]* *Dongsheng Wen[2,6]**

[1]School of Energy and Environmental Engineering, University of Science and Technology Beijing, Beijing 100083, China

[2]School of Aeronautic Science and Engineering, Beihang University, Beijing 100191, China

[3]SHENYUAN Honors College, Beihang University, Beijing 100191, China

[4]School of Mechanical Engineering and Automation, Harbin Institute of Technology, Shenzhen 518055, China

[5]Department of Energy and Power Engineering, Tsinghua University, Beijing 100084, China

[6]School of Chemical and Process Engineering, University of Leeds, Leeds LS2 9JT, UK

ABSTRACT: Although a superhydrophobic surface could realize rapid rebounding (*i.e.*, short contact time) of an orthogonal impacting droplet, the rebounding along the original impacting route may limit its engineering application; in contrast, the directional transportation seems to be more promising. Here, we achieve directional transportation of a droplet impacting on a wettability-controlled surface. When the droplet eccentrically impacts on the boundary between the superhydrophobic part and the hydrophilic part, it undergoes spreading, retracting, departure, throwing and breaking up stages, and finally bounces off directionally. The directional transportation distance could even reach more than ten times of the droplet size, considered the adhesion length (*i.e.*, covering length on the hydrophilic part by the droplet at the maximum spreading) is optimized. However, there is a critical adhesion length, above which the directional transportation does not occur. To be more generalized, the adhesion length is de-dimensionalized by the maximum spreading radius, and the results show that as the dimensionless adhesion length increases, the transportation distance first increases and then decreases to zero. Under the present impacting conditions, the optimal dimensionless adhesion length corresponding to the maximum transportation distance is near 0.4, and the critical dimensionless adhesion length is about 0.7. These results provide fundamental understanding of droplet directional transportation, and could be useful for related engineering applications.

KEYWORDS: droplet impacting; wettability control; superhydrophobic; directional transportation; adhesion length.

INTRODUCTION

Droplet impacting is ubiquitous either in nature, *e.g.*, raindrops falling, or in industrial processes such as aircraft icing, water harvesting, electricity generation and spray cooling.[1-5] As a droplet-surface interaction phenomenon, the droplet impacting is affected by surface structures and wettability greatly, presenting various outcomes including deposition, splashing, and rebound.[6-10] Specially, the rebound of droplets when impacting on nanoengineered superhydrophobic surfaces has attracted numerous attention in recent decades,[11-15] as it has promising applications in various engineering fields such as anti-icing, self-cleaning, and fluid transportation.[16-21]

For droplet impacting on a superhydrophobic surface, the contact time, *i.e.*, the rebound time, is a key factor which influences the practical application significantly.[22] For example, if the contact time is short enough that a supercooled droplet can bounce off from aircraft wings before ice nucleation appears, effective anti-icing could be

achieved.[2, 17] The contact time is limited to $\sim 2.6\tau_0$ (τ_0 is the inertial-capillary time, $(\rho r^3/\sigma)^{1/2}$, where ρ is the fluid density, r is the impacting droplet radius and σ is the fluid surface tension) for the droplet impacting on a flat superhydrophobic surface.[22-23] Thus, many efforts have been paid to reduce the contact time. Bird $et\ al.$ reported that the addition of macrotextures on superhydrophobic surfaces could alter the impacting droplet dynamics by redistributing the droplet mass, and then reduce the contact time by 37% compared with the droplet impacting on flat surfaces.[24] Liu $et\ al.$ fabricated a superhydrophobic surface patterned with lattices of posts decorated with nanotextures and observed a special rebound regime on this surfaces, $i.e.$, the pancake bouncing, that the droplet bounces off from the surface at the spreading stage.[25] The pancake bouncing is very counter-intuitive and can extremely reduce the contact time by 80%.[25] In addition to these, other types of superhydrophobic surfaces, such as the curved surface, the anisotropic surface and the surface with cavities, were also reported to be effective for the reduction of contact time.[23, 26-33]

However, if the superhydrophobic surface is horizontally located, the contact time may not be that crucial, because no matter how short the contact time, the rebounding droplet finally falls back to the surface under gravity. Also take the anti-icing application as an example, obviously, the directional transportation rather than the perpendicular rebound of the impacting droplet is wanted on this condition. However, the directional transportation behavior of impacting droplet is less noticed with very few research reported. Schutzius $et\ al.$ designed a hydrophilic arc on a superhydrophobic surface and realized non-orthogonal rebounding when the droplet impacts the center of the arc.[34] Similarly, Song $et\ al.$ reported gyrating, rolling and lateral deflection of impacting droplets through heterogeneous surface wettability regulation very recently.[35] In their another work, they further quantitatively investigated the lateral deflection and revealed the correlation between the lateral momentum of rebounding droplets and the surface area of a geometric region that depends on the position-coupling between the droplet maximum spreading and the wettability pattern.[36] Utilizing topographically patterned surfaces to generate two concurrent thermal states (Leidenfrost and contact-boiling) of one hot impacting droplet, Li $et\ al.$ also achieved directional transport of high temperature droplets.[37] The above works have presented the prior results of the directional transportation of impacting droplets and emphasized its importance, but targeted research is far from enough with many core problems remaining unsolved. In other words, due to the complexity of the droplet morphology evolution and the milliseconds-scale droplet-surface interaction, it is still a challenge to achieve precise and controllable directional transportation of impacting droplets currently.

In the present work, we fabricate a wettability-controlled surface, one-half of which exhibits superhydrophobic property while the other half is hydrophilic, and report that the directional transportation of droplet can be realized when the droplet impacts on the boundary between the superhydrophobic part and the hydrophilic one. The maximum directional transport distance could even reach several ten times of the impacting droplet radius, indicating a rather effective directional transportation. Furthermore, via tuning the impacting location, the directional transport distance and the rebounding angle can be controlled precisely. These results constitute a significant step in the advances of directional transportation of impacting droplets and present fresh insights into related engineering applications such as anti-icing, water harvesting and self-cleaning.

EXPERIMENTAL SECTION

Wettability-controlled surfaces

The experimental surface is a wettability-controlled surface with half of it being superhydrophobic and the rest being unprocessed aluminum substrate, as shown in Fig. 1. The superhydrophobic part is fabricated by the chemical deposition-etching method and is covered with flower-like structures.[38] The static, advancing, and receding contact angles of the superhydrophobic part are 159.8±1.4º, 163.4±2.7º, and 157.2±3.1º, respectively. The other part of the experimental surface, *i.e.*, the unprocessed aluminum substrate, is flat and hydrophilic with static, advancing, and receding contact angles of 85.6±1.6º, 112.6±2.3º, and 56.4±2.9º, respectively. Similar to our previous research,[38-39] the contact angles are measured using 2 μL deionized water droplets at room temperature (25ºC) using a measurement equipment (Biolin Theta Lite, Finland), and all the standard deviations are based on two parallel surfaces, with five measurements for each.
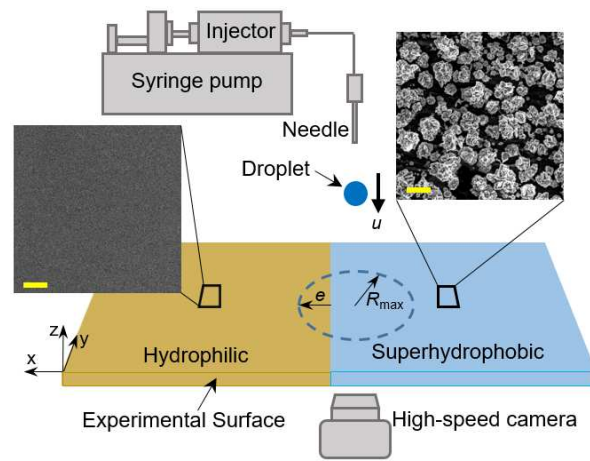
Figure 1. Schematic of experimental surfaces, of which one half is superhydrophobic with flower-like structures and the other half is hydrophilic without obvious micro structure, and schematic of experimental system, which mainly contains a droplet production module and a high-speed camera module. The scale bar in the SEM (scanning electron microscope) images is 10 μm.

Experimental setup and operation

The experimental system mainly contains a droplet production module and a high-speed camera module, as shown in Fig. 1. The droplet production module is composed of a syringe pump, an injector and a micro needle (0.31 mm diameter), and the high-speed camera module contains a high-speed camera (PCO. Dimax HS4, Germany), a light source and a high-performance computer. During the experiments, the experimental surface is horizontally located on a XYZ-freedom platform. The droplet with a certain diameter is produced and falling under gravity until it impacts on the boundary between the superhydrophobic part and the hydrophilic part of the experimental surface (the dash line in Fig. 1 represents the maximum spreading, which has a radius of R_{max}). The whole impacting process is recorded by the high-speed camera. The droplet diameter (d), impacting velocity (u), and the adhesion length (e) are varied in the experiments. The adhesion length, e, is defined as the parallel distance from the boundary to the

triple phase contact line on the hydrophilic part when the droplet has the maximum spreading radius, R_{max}, as shown in Fig. 1, Fig. 2(a) and Fig. 5(a). It can also be described as the covering length by the spreading droplet on the hydrophilic part when reaching the maximum spreading.

RESULTS AND DISCUSSION

Impacting droplet morphology and directional transportation mechanism

Droplet impacting on a homogeneous superhydrophobic surface has been widely studied, and the typical dynamic process can be divided into three stages: spreading, retracting and rebounding.[7, 40] By contrast, the impacting dynamics on a wettability-controlled surface are different. Figure 2 shows time-lapse images of droplet impacting on the wettability-controlled experimental surface under conditions of d=2.1 mm, u=1.5 m/s, and e=1.0 mm from side-view and top-view. See Video S1 in the Supporting Information for multimedia. As Fig. 2 shown, after the droplet impacts, the droplet first spreads to a circular film under inertial force and reaches the maximum spreading (side-view image at 5.4 ms or top-view image at 4.0 ms), which is similar to the spreading on a regular homogeneous surface.[41-44] At the maximum spreading, the circular film covers both the hydrophilic part and the superhydrophobic part of the experimental surface with an adhesion length (e) of 1 mm. Then, the film begins to retract. The retracting stage is strongly affected by surface wetting property that only water film on the superhydrophobic part retracts towards the impact point while water film on the hydrophilic part adheres and gets pinned (side-view image at 8.1 ms or top-view image at 6.0 ms). At some moment, the water film on the superhydrophobic part finishes the retraction and totally departs from the surface, while the water film on the hydrophilic part still keeps pinned. The pinned water just behaves like a "pivot", and the rebounding, spindly water behaves like a "string", towing itself to rotate around the "pivot". During the rotation, the centripetal force breaks the "string", in other words, the rotating part of water breaks up with the pinned water and continues to fly in the air, doing parabolic motion (see the side-view images from 23.8 ms to 80 ms). This is very similar to a droplet throwing process, and the throwing distance from the impact point to the landing point is the droplet directional transportation distance, labelled as X. In Fig. 2, the directional transportation distance is measured to be ~ 28 mm, which is 13 times longer than the droplet diameter, indicating a remarkable directional transportation.
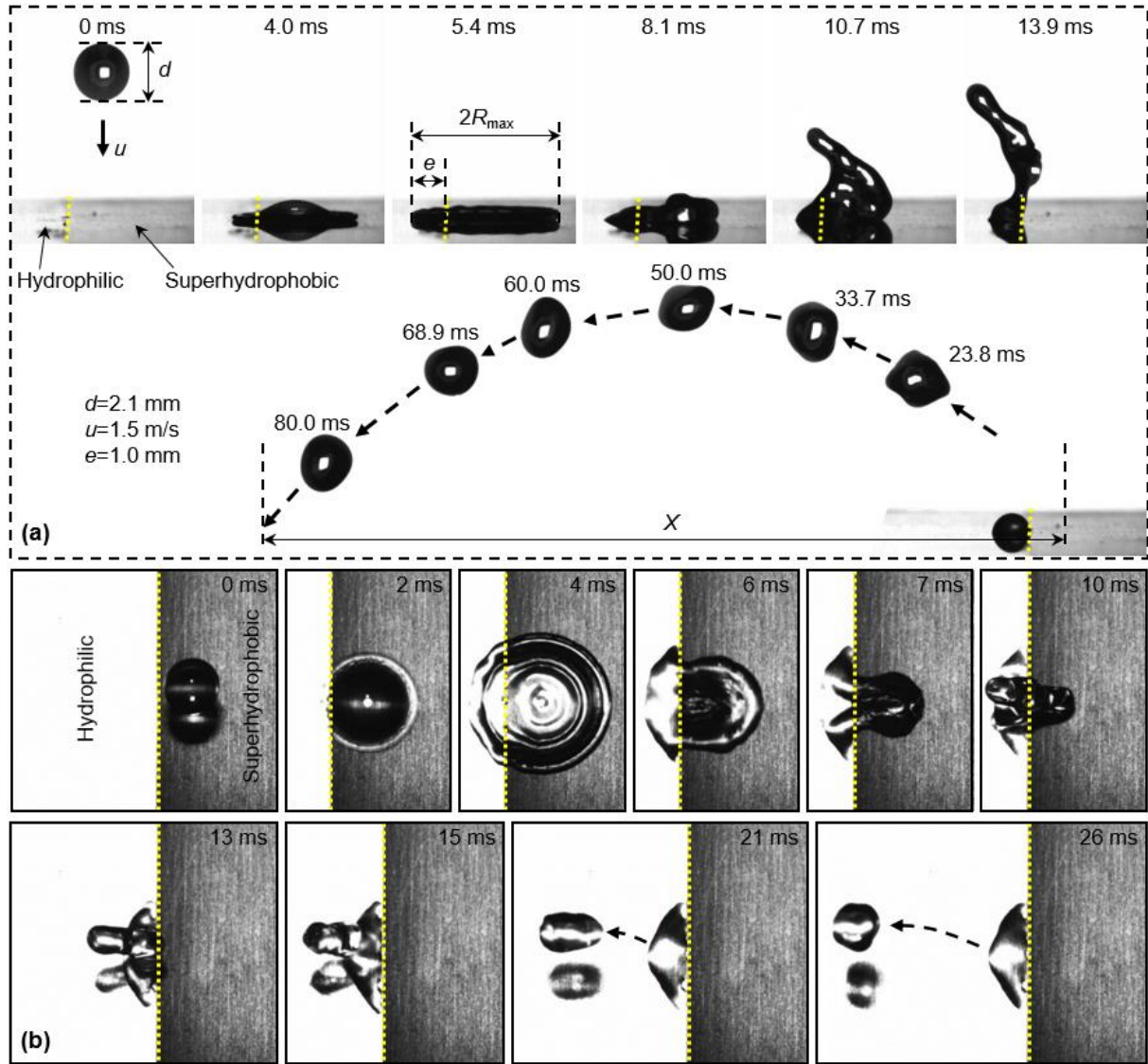
Figure 2. (a) Side-view and (b) top-view images of droplet impacting on the wettability-controlled experimental surface under conditions of d=2.1 mm, u=1.5 m/s, and e=1.0 mm. In these images, the yellow dashed line represents the boundary between the hydrophilic part and the superhydrophobic part. As seen, the droplet flies away laterally in the form of parabolic motion, after vertically impacting on the wettability-controlled surface (See Video S1 in the Supporting Information for multimedia). The directional transportation distance (X) is 13 times longer than the droplet diameter (d). It should be noted that the side-view and top-view images are taken separately (we only have one high-speed camera) so their time series are not strictly corresponding to each other, but the impacting conditions are exactly the same.

To further understand the directional transportation mechanism of the impacting droplet, we further conducted a Proof of Principle simulation based on the Volume of Fluid (VOF) method. Coupled with the VOF method, the continuum surface force (CSF) model is used to calculate the surface tension and the Kistler's model is adopted to address the dynamic contact angle issue. Because the simulation is just Proof of Principle, we will not introduce

more about the simulation method here, and please see more details about the simulation method in our previous work.[45] As shown in Fig. 3, according to the droplet morphology evolution, six stages are divided during the droplet impacting on the wettability-controlled surface, including spreading, retracting, departure, throwing, breaking up, and flight. In addition, the velocity vectors inside the droplet at every stage are also marked for the motion trend analysis. As seen in Fig. 3(a), the wettability-controlled surface does not affect the spreading stage because the spreading is dominated by the inertial force. At the retracting stage shown in Fig. 3(b), the droplet behavior is affected greatly by surface wettability that lateral velocity vectors inside the water film on the superhydrophobic are formed towards the hydrophilic part. Moreover, these lateral velocity vectors will not disappear in the subsequent stages. It should be emphasized that the retracting stage is the key stage for the formation of lateral velocity vectors, because a lateral force is generated due to the receding contact angle difference between the hydrophilic and the superhydrophobic part of the wettability-controlled surface. At the end of the retracting stage, the water rebounds from the superhydrophobic part obliquely but the water on the hydrophilic part is still pinned, as shown in Fig. 3(c). Then, at the throwing stage shown in Fig. 3(d), the pinned water serves as a "pivot" and the rebounding water rotates around it under the action of centripetal force. The centripetal force breaks the rotating water at some moment and the separated droplet continues to fly in the air, as shown in Figs. 3(e) and (f).
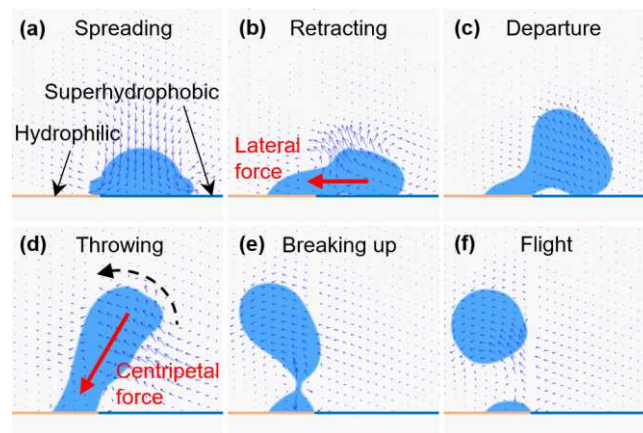
Figure 3. Schematic of droplet impacting on the wettability-controlled surface, during which six stages are divided, including (a) spreading, (b) retracting, (c) departure, (d) throwing, (e) breaking up, and (f) flight. According to the numerical results by VOF method, the velocity vectors inside a droplet slice in X-Z plane are also marked with blue arrows. These velocity vectors indicate that the lateral velocity is generated at the retracting stage.

Figure 4 shows the variations of the droplet contact line position (X-axis) with time at the spreading and retracting stages under conditions of d=2.1 mm and u=1.5 m/s. At the spreading stage, droplet on the hydrophilic part and the superhydrophobic part behaves similarly and reaches the maximum spreading at the same time. However, the contact line moves differently on the two parts at the retracting stage, which has been mentioned above. On the hydrophilic part, the contact line gets pinned and remains at the same position after it reaches the

maximum spreading; on the superhydrophobic part, the contact line begins to recede after reaching a maximum value until it decreases to zero (departure from the surface). This is consistent with the images shown in Fig. 2. In addition, the contact line variation is similar for different adhesion lengths, which means that the droplet impacting position makes no difference on the contact line variation. Figure 4 also shows that, the contact line varies almost linearly with time at the retraction stage, indicating that the retraction rate on the superhydrophobic part is constant.
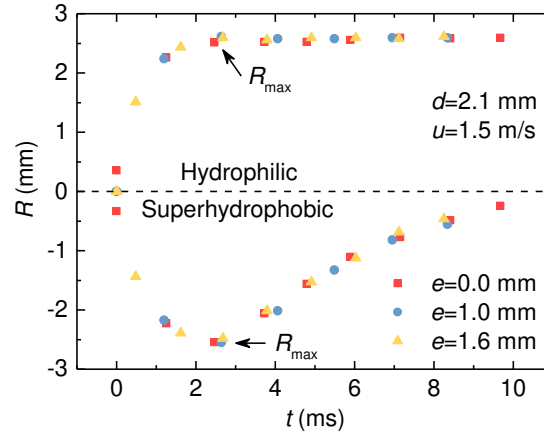
Figure 4. Variation of the contact line position (X-axis) of the impacting droplet on the wettability-controlled experimental surface under conditions of d=2.1 mm and u=1.5 m/s. Assuming that the X-axis value of the impacting point is zero. As seen, the contact line variations are consistent for different adhesion lengths, e. In addition, on the hydrophilic part of the experimental surface, the contact line is pinned after reaching the maximum spreading, while on the superhydrophobic part, the contact line continues to retract until the droplet departs from the surface.

Lateral velocity and transportation distance

As mentioned above, the retracting stage is the key stage for the directional transportation, because a lateral force is generated at the retracting stage (see Fig. 3(b)); therefore, mechanical analysis on the contact line is made at the retracting stage. In the mechanical model, we assume that, (i) water film on the superhydrophobic part retracts toward the impacting point, (ii) the retraction rate of the water film contact line on the superhydrophobic part is constant, and (iii) the dynamic contact angles during retracting are unvaried on both the hydrophilic part and the superhydrophobic part and regarded as the receding contact angle for convenience. Actually, images from 4 ms to 7 ms in Fig. 2(b) support the assumption (i), and the contact line position data in Fig. 4 supports the assumption (ii). Figure 5(a) shows a schematic of the droplet contact line at a certain time at the retracting stage on the wettability-controlled surface. Based on these assumptions, the lateral force applied on the contact line towards the hydrophilic part (X-axis direction) can be expressed as

$$F = \sigma L\left(cos\theta_{phi,r} - cos\theta_{pho,r}\right) \tag{1}$$

where σ is the surface tension of water; $\theta_{phi,r}$ is the receding contact angle of the hydrophilic part and $\theta_{pho,r}$ is the

receding contact angle of the superhydrophobic part; L, the length of the yellow solid line in Fig. 5(a), is the characteristic length for force, and it varies with time, τ. Because the retraction rate of the contact line on the superhydrophobic part is assumed to be constant, the radius of the contact line is calculated as, $R=R_{max}(1-\tau/t)$. Thus, according to the geometrical relationship, L is given by

$$L = 2R_{max}\sin\varphi\left(1-\frac{\tau}{t}\right) \tag{2}$$

where R_{max} is the water film radius at the maximum spreading; t is the total retracting time for the water film on the superhydrophilic part; φ is the characteristic angle, which only relates to the impacting conditions and the impacting point, $i.e.$, e and R_{max},

$$\sin\varphi = \frac{\sqrt{2R_{max}e-e^2}}{R_{max}} \tag{3}$$

where e is the adhesion length. Substituting Eqs. (2) and (3) into Eq. (1) gives

$$F = 2\sigma\sqrt{2R_{max}e - e^2}\left(\cos\theta_{phi,r} - \cos\theta_{pho,r}\right)\left(1-\frac{\tau}{t}\right) \tag{4}$$

According to the theorem of momentum, change in momentum can be obtained by integrating Eq. (4) in time. After divided by the droplet mass, the lateral velocity of the droplet is expressed as

$$v_x = \frac{6\sigma\sqrt{2R_{max}e-e^2}\left(\cos\theta_{phi,r}-\cos\theta_{pho,r}\right)t}{\pi d^3\rho} \tag{5}$$

As seen in Eq. (5), the lateral velocity mainly relates to the impacting conditions and the surface contact angles.

To validate the reliability of Eq. (5), we extract the lateral velocities from the time-lapse images in the droplet impacting experiments with various adhesion lengths on the wettability-controlled surface. The extracted results are presented in Fig. 5(b). Error bars in Fig. 5(b) or other figures display the standard deviations of parallel measurements. As seen, the lateral velocity increases with increasing adhesion length, in other words, the closer the impact point to the boundary between the hydrophilic and superhydrophobic part, the greater the lateral velocity. The predicted results by Eq. (5) are also exhibited in Fig. 5(b), which are in good agreement with the experimental value. However, when the adhesion length exceeds a critical value, the droplet cannot fly away directionally. Under the current conditions that $d=2.1$ mm and $u=1.5$ m/s, the critical value is about 2 mm. This can be interpreted as the following reason. When the adhesion length exceeds the critical value, the volume of the rotating water at the throwing stage is so small that the surface tension overcomes the centripetal force and the rotating part prefers to merge with the pinning water instead of flying away. Thus, the directional transportation does not take place anymore. However, it is still a great challenge to quantitatively predict the critical adhesion length, and the current model cannot do that, so more effort is still needed.
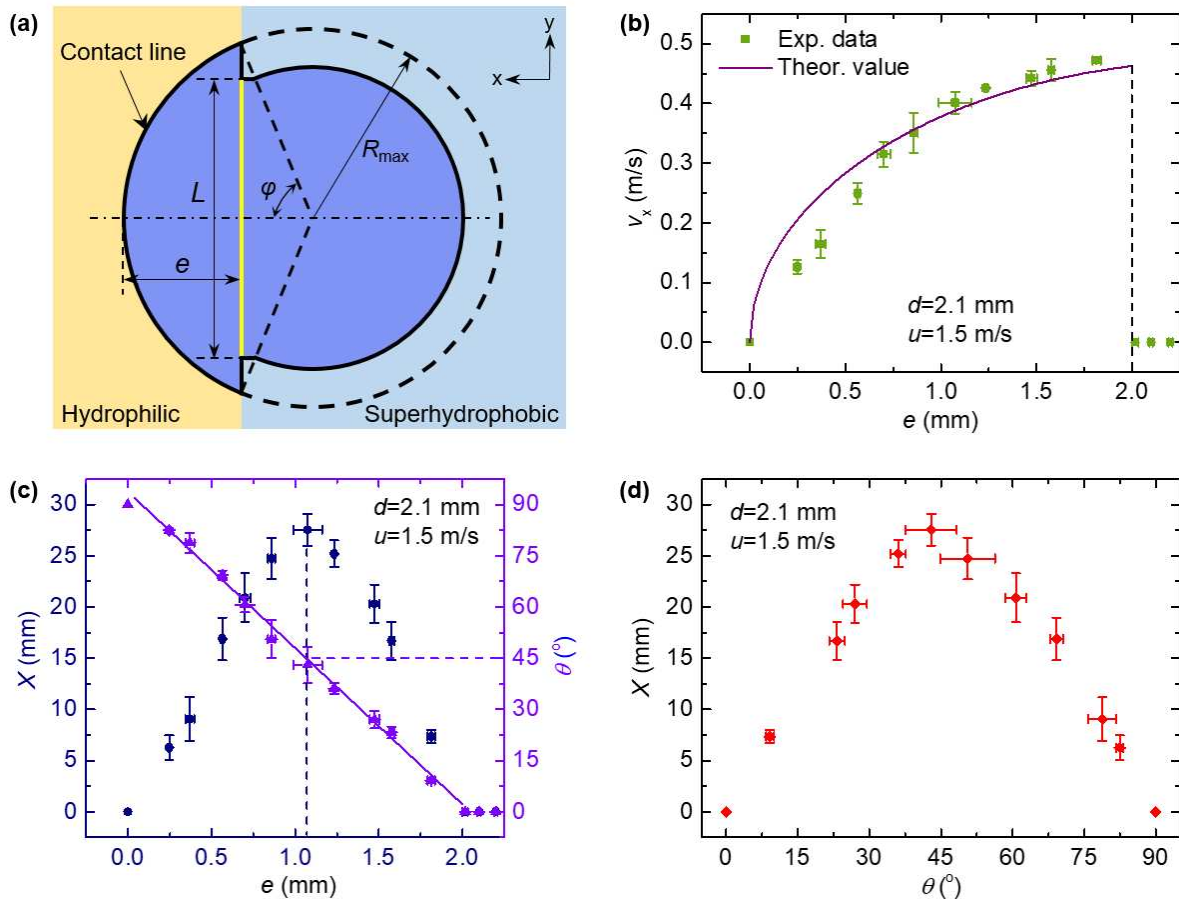
Figure 5. (a) Force analysis on the contact line of the impacting droplet at the retracting stage. *L*, the length of the yellow solid line, is the characteristic length for force, and it varies with time. φ is the characteristic angle, which only relates to the impacting conditions and the impacting point, *i.e.*, *e* and R_{max}. (b) Experimental and predicted lateral velocities of the droplet versus adhesion length under conditions of *d*=2.1 mm and *u*=1.5 m/s. As the adhesion length increases, the lateral velocity increases, but when the adhesion length exceeds a critical value, the lateral velocity becomes zero and the droplet does not fly away directionally anymore. (c) Relation between the transportation distance (and the throwing angle) and the adhesion length under conditions of *d*=2.1 mm and *u*=1.5 m/s. There is an optimal adhesion length to achieve the longest transportation distance. In addition, as the adhesion length increases, the throwing angle decreases linearly. (d) Relation between the transportation distance and the throwing angle. The transportation distance is longest when the throwing angle is 45º.

Beside the lateral velocity, the transportation distance, *X*, is also an important parameter. Figure 5(c) shows the relation between the directional transportation distance and the adhesion length under conditions of *d*=2.1 mm and *u*=1.5 m/s. It can be found that the transportation distance increases first and decreases later with increasing adhesion length. There is an optimal adhesion length when the transportation distance reaches the maximum value. Under the current conditions, this optimal adhesion length is near 1 mm. We also extract the droplet throwing angle at the breaking up stage from the experiments, and show the results in Fig. 5(c). As seen, the throwing angle varies linearly from 90º to 0º as the adhesion length increases. The 90º throwing angle means vertical rebounding from the

superhydrophobic part and the 0° throwing angle implies that the droplet cannot fly away anymore. In addition, when the transportation distance reaches the maximum, the corresponding throwing angle is just 45°. The relation between the directional transportation distance and the throwing angle in Fig. 5(d) shows this conclusion more clearly. In other words, when reaching the maximum transportation distance, the droplet lateral velocity is not its maximum value corresponding to the critical adhesion length, while the optimal adhesion length corresponds to the 45° throwing angle. This is because that the directional transportation of impacting droplet on the wettability-controlled surface is a parabolic movement in plane, and it satisfies the basic parabolic law that the projection distance is equal to $(v^2\sin2\theta)/g$, where v is the projectile velocity, θ is the throwing angle and g is acceleration of gravity. Based on the parabolic law, when the throwing angle is 45°, the transportation distance is the longest and the adhesion length is optimal.

It should be specified that there is a reduction of mass in the directional transportation on the wettability-controlled surface because the water on the hydrophilic part will adhere to the surface without flying away. Therefore, the investigation on the residual water is necessary. However, we have to admit that we cannot measure the residual water mass accurately because the residual water has quite irregular shape, but we can estimate it. As shown in the top-view images in Fig. 6(a), after comparing the size of the water on the hydrophilic part at the maximum spreading and the residual water, we found that these two water sizes are almost the same. Thus, we can use the water size covering the hydrophilic part at the maximum spreading to estimate the residual water size, *i.e.*, the area ratio of arched water film covering the hydrophilic part to the whole water film at the maximum spreading could be approximately regarded as the mass ratio of the residual water to the whole droplet. Figure 6(b) shows these estimated mass ratios with increasing adhesion lengths under conditions of d=2.1 mm and u=1.5 m/s. As seen, when the adhesion length is smaller than the critical value, the mass ratio increases almost linearly, while it suddenly become one when the adhesion length exceeds the critical value since the directional transportation disappears and the whole droplet adheres on the surface.
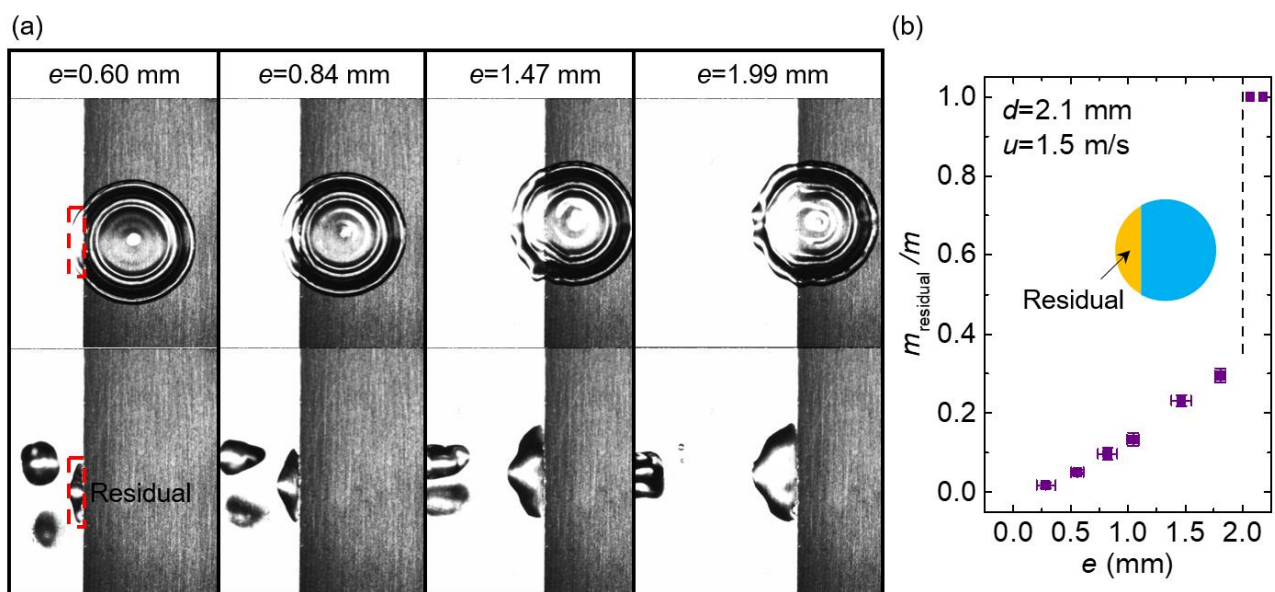
Figure 6. (a) Size comparison of the water film on the hydrophilic part at the maximum spreading and the residual

water under conditions of d=2.1 mm and u=1.5 m/s. The red dashed boxes mark an example when the adhesion length is 0.60 mm. As seen, these two water sizes are almost the same. Therefore, we can use the water size covering the hydrophilic part at the maximum spreading to estimate the residual water size. (b) The estimated mass ratio of the residual water to the whole water. Before the critical adhesion length, the mass ratio is nearly linear, and after the critical adhesion length, the mass ratio becomes one because the directional transportation cannot happen.

Effects of impacting conditions

To clarify the dependence of directional transportation distance on the impacting conditions, droplet impacting experiments on the wettability-controlled surface with different droplet diameters and impacting velocities are conducted. To be more generalized, we use the dimensionless adhesion length, e/R_{max}, and the dimensionless directional transportation distance, X/d, in Fig. 7. Figure 7(a) shows how the impacting velocities, including 1.2 m/s, 1.5 m/s, and 1.9 m/s, affect the transportation distance when the droplet diameter remains unchanged at d=2.1 mm. As seen, the dimensionless transportation distance increases as the impacting velocity increases. Besides, the optimal dimensionless adhesion length which corresponds to the maximum transportation distance also increases with increasing impacting velocity, but this increasing is slight. Figure 7(b) shows how the droplet diameters, including 2.1 mm, 2.4 mm, and 2.8 mm, affect the directional transportation distance when the impacting velocity keeps constant. The result shows that as the droplet diameter increases, the dimensionless transportation distance decreases but the optimal dimensionless adhesion length does not change obviously, and is basically about 0.4. In addition, Figure 7 also shows the critical dimensionless adhesion lengths under current impacting conditions. Roughly when the dimensionless adhesion length is larger than 0.7 the directional transportation of the impacting droplet on the wettability-controlled surface does not happen anymore. These results about the optimal adhesion length and the critical adhesion length constitute a significant step into how to achieve precise and controllable directional transportation of impacting droplets.
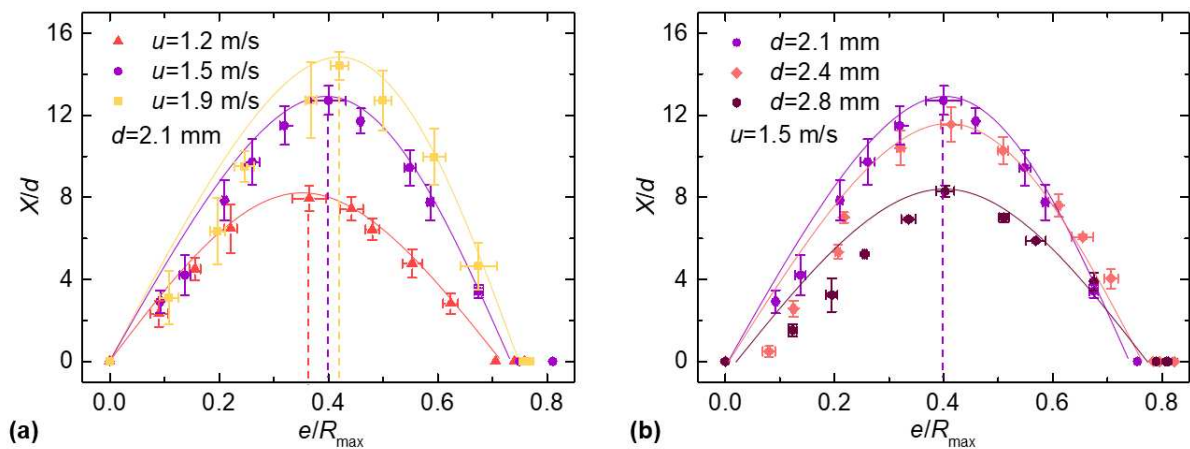
Figure 7. (a) The effect of the impacting velocity on the dimensionless directional transportation distance (X/d) and the optimal dimensionless adhesion length (e/R_{max}) under constant droplet diameter. With increasing

impacting velocity, the dimensionless transportation distance increases; the optimal dimensionless adhesion length also increases slightly. (b) The effect of the droplet diameter on the dimensionless directional transportation distance (X/d) and the optimal dimensionless adhesion length ($e/R_{\max}$) under constant impacting velocity. Reducing the droplet diameter is beneficial for the increase of the dimensionless transportation distance, but the droplet diameter does not obviously affect the optimal dimensionless adhesion length.

CONCLUSION

In summary, we fabricate a wettability-controlled surface with one-half superhydrophobic and the other half hydrophilic, and achieve directional droplet transportation by impacting a droplet on the boundary between the superhydrophobic part and the hydrophilic part. Under the present impacting conditions, the directional transportation distance can reach more than ten times of the droplet size through reasonable regulation. According to the droplet morphology evolution, the directional transportation process is divided into six stages including spreading, retracting, departure, throwing, breaking up, and flight stages, of which the retracting stage is the key stage for the directional transportation. During the retracting stage, a net lateral force is generated on the droplet contact line due to the wettability difference between the hydrophilic part and the superhydrophobic part. A mechanical model is developed to calculate lateral force and to predict the lateral velocity, which has been validated by the experiments. The lateral velocity increases with increasing adhesion length, but there is critical adhesion length above which the directional transportation disappears. As for the transportation distance, it first increases and then decreases with increasing adhesion length and when the transportation distance reaches the maximum value the throwing angle at the breaking up stage is 45°, which satisfies the basic parabolic laws. Besides, we found that the throwing angle decreases linearly with increasing adhesion length. Under the present impacting conditions, the optimal dimensionless adhesion length corresponding to the maximum transportation distance is near 0.4, and the critical dimensionless adhesion length corresponding to the disappearing transportation is about 0.7. However, the wettability-controlled surface cannot achieve complete droplet transportation because part of the impacting droplet still adheres to the hydrophilic side of the surface and the residual mass increases with increasing adhesion length before the critical value. In the field of droplet transportation and regulation, this work takes a big step forward, but there is still much work to be done, such as building a more comprehensive model to predict the optimal and the critical dimensionless adhesion length, broadening the impacting conditions to obtain more experimental data, and conducting more accurate simulations to explain the fluid dynamics.

ASSOCIATED CONTENT
Supporting information
Side-view video of the directional transportation of impacting droplets on wettability-controlled surfaces (Video S1.MP4)

AUTHOR INFORMATION

Corresponding Authors

*E-mail: chu_fuqiang@126.com

*E-mail: d.wen@buaa.edu.cn

Author Contributions

‡F. Chu and J. Luo contributed equally to this work. The manuscript was written through contributions of all authors. All authors have given approval to the final manuscript.

ORCID

Fuqiang Chu: 0000-0002-4054-143X

Xiaomin Wu: 0000-0001-7703-0038

Dongsheng Wen: 0000-0003-3492-7982

Notes

The authors declare no competing financial interest.

REFERENCES

[1]   Josserand, C.; Thoroddsen, S. T., Drop Impact on a Solid Surface. *Annu. Rev. Fluid Mech.* **2016,** *48* (1), 365-391.

[2]   Mishchenko, L.; Hatton, B.; Bahadur, V.; Taylor, J. A.; Krupenkin, T.; Aizenberg, J., Design of ice-free nanostructured surfaces based on repulsion of impacting water droplets. *ACS Nano* **2010,** *4* (12), 7699-7707.

[3]   Wang, X.; Zeng, J.; Yu, X.; Zhang, Y., Superamphiphobic coatings with polymer-wrapped particles: enhancing water harvesting. *J. Mater. Chem. A* **2019,** *7* (10), 5426-5433.

[4]   Xu, W.; Zheng, H.; Liu, Y.; Zhou, X.; Zhang, C.; Song, Y.; Deng, X.; Leung, M.; Yang, Z.; Xu, R. X.; Wang, Z. L.; Zeng, X. C.; Wang, Z., A droplet-based electricity generator with high instantaneous power density. *Nature* **2020,** *578*, 392-396.

[5]   Kim, J., Spray cooling heat transfer: The state of the art. *Int. J. Heat Fluid Flow* **2007,** *28* (4), 753-767.

[6]   Roisman, I. V.; Lembach, A.; Tropea, C., Drop splashing induced by target roughness and porosity: The size plays no role. *Adv. Colloid Interface Sci.* **2015,** *222*, 615-621.

[7]   Khojasteh, D.; Kazerooni, M.; Salarian, S.; Kamali, R., Droplet impact on superhydrophobic surfaces: A review of recent developments. *J. Ind. Eng. Chem.* **2016,** *42*, 1-14.

[8]   Antonini, C.; Amirfazli, A.; Marengo, M., Drop impact and wettability: From hydrophilic to superhydrophobic surfaces. *Phys. Fluids* **2012,** *24* (10), 102104.

[9] Tang, C.; Qin, M.; Weng, X.; Zhang, X.; Zhang, P.; Li, J.; Huang, Z., Dynamics of droplet impact on solid surface with different roughness. *Int. J. Multiph. Flow* **2017,** *96*, 56-69.

[10] Lin, S.; Zhao, B.; Zou, S.; Guo, J.; Wei, Z.; Chen, L., Impact of viscous droplets on different wettable surfaces: Impact phenomena, the maximum spreading factor, spreading time and post-impact oscillation. *J. Colloid Interface Sci.* **2018,** *516*, 86-97.

[11] Cao, M.; Guo, D.; Yu, C.; Li, K.; Liu, M.; Jiang, L., Water-Repellent Properties of Superhydrophobic and Lubricant-Infused "Slippery" Surfaces: A Brief Study on the Functions and Applications. *ACS Appl. Mater. Interfaces* **2016**, *8* (6), 3615-3623.

[12] Wang, Y.; Xue, J.; Wang, Q.; Chen, Q.; Ding, J., Verification of icephobic/anti-icing properties of a superhydrophobic surface. *ACS Appl. Mater. Interfaces* **2013**, *5* (8), 3370-3381.

[13] Maitra, T.; Antonini, C.; Tiwari, M. K.; Mularczyk, A.; Imeri, Z.; Schoch, P.; Poulikakos, D., Supercooled Water Drops Impacting Superhydrophobic Textures. *Langmuir* **2014,** *30* (36), 10855-10861.

[14] Liu, Y.; Yan, X.; Wang, Z., Droplet dynamics on slippery surfaces: small droplet, big impact. *Biosurf. Biotribol.* **2019,** *5* (2), 35-45.

[15] Yamauchi, Y.; Tenjimbayashi, M.; Samitsu, S.; Naito, M., Durable and Flexible Superhydrophobic Materials: Abrasion/Scratching/Slicing/Droplet Impacting/Bending/Twisting-Tolerant Composite with Porcupinefish-Like Structure. *ACS Appl. Mater. Interfaces* **2019**, *11* (35), 32381-32389.

[16] Hao, T.; Wang, K.; Chen, Y.; Ma, X.; Lan, Z.; Bai, T., Multiple Bounces and Oscillatory Movement of a Microdroplet in Superhydrophobic Minichannels. *Ind. Eng. Chem. Res.* **2018,** *57* (12), 4452-4461.

[17] Lv, J.; Song, Y.; Jiang, L.; Wang, J., Bio-inspired strategies for anti-icing. *ACS Nano* **2014,** *8* (4), 3152-69.

[18] Lu, Y.; Sathasivam, S.; Song, J.; Crik, C. R.; Carmalt, C. J.; Parkin, I. P., Robust self-cleaning surfaces that function when exposed to either air or oil. *Science* **2015,** *347*, 1132-1135.

[19] Shen, Y.; Wu, X.; Tao, J.; Zhu, C.; Lai, Y.; Chen, Z., Icephobic materials: Fundamentals, performance evaluation, and applications. *Prog. Mater. Sci.* **2019,** *103*, 509-557.

[20] Hao, C.; Li, J.; Liu, Y.; Zhou, X.; Liu, Y.; Liu, R.; Che, L.; Zhou, W.; Sun, D.; Li, L.; Xu, L.; Wang, Z., Superhydrophobic-like tunable droplet bouncing on slippery liquid interfaces. *Nat. Commun.* **2015,** *6*, 7986.

[21] Li, J.; Qin, Q. H.; Shah, A.; Ras, R. H. A.; Tian, X.; Jokinen, V., Oil droplet self-transportation on oleophobic surfaces. *Sci. Adv.* **2016,** *2*, e1600148.

[22] Richard, D.; Clanet, C.; David, Q., Surface phenomena: Contact time of a bouncing drop. *Nature* **2002,** *417*, 811.

[23] Gauthier, A.; Symon, S.; Clanet, C.; Quéré, D., Water impacting on superhydrophobic macrotextures. *Nat.Commun.* **2015,** *6* (1),8001.

[24] Bird, J. C.; Dhiman, R.; Kwon, H. M.; Varanasi, K. K., Reducing the contact time of a bouncing drop. *Nature* **2013,** *503* (7476), 385-388.

[25] Liu, Y.; Moevius, L.; Xu, X.; Qian, T.; Yeomans, J. M.; Wang, Z., Pancake bouncing on superhydrophobic surfaces. *Nat. Phys.* **2014,** *10* (7), 515-519.

[26] Liu, Y.; Andrew, M.; Li, J.; Yeomans, J. M.; Wang, Z., Symmetry breaking in drop bouncing on curved surfaces. *Nat. Commun.* **2015,** *6*, 10034.

[27] Lv, C.; Hao, P.; Zhang, X.; He, F., Drop impact upon superhydrophobic surfaces with regular and hierarchical roughness. *Appl. Phys. Lett.* **2016,** *108* (14), 141602.

[28] Zhang, R.; Hao, P.; He, F., Rapid Bouncing of High-Speed Drops on Hydrophobic Surfaces with Microcavities. *Langmuir* **2016,** *32* (39), 9967-9974.

[29] Song, M.; Liu, Z.; Ma, Y.; Dong, Z.; Wang, Y.; Jiang, L., Reducing the contact time using macro anisotropic superhydrophobic surfaces — effect of parallel wire spacing on the drop impact. *NPG Asia Mater.* **2017,** *9* (8), e415-e415.

[30] Shen, Y.; Liu, S.; Zhu, C.; Tao, J.; Chen, Z.; Tao, H.; Pan, L.; Wang, G.; Wang, T., Bouncing dynamics of impact droplets on the convex superhydrophobic surfaces. *Appl. Phys. Lett.* **2017,** *110* (22), 221601.

[31] Lin, D.-J.; Wang, L.; Wang, X.-D.; Yan, W.-M., Reduction in the contact time of impacting droplets by decorating a rectangular ridge on superhydrophobic surfaces. *Int. J. Heat Mass Transfer.* **2019,** *132*, 1105-1115.

[32] Weisensee, P. B.; Ma, J.; Shin, Y. H.; Tian, J.; Chang, Y.; King, W. P.; Miljkovic, N., Droplet impact on vibrating superhydrophobic surfaces. *Phys. Rev. Fluids* **2017,** *2* (10), 103601.

[33] Chantelot, P.; Mazloomi Moqaddam, A.; Gauthier, A.; Chikatamarla, S. S.; Clanet, C.; Karlin, I. V.; Quere, D., Water ring-bouncing on repellent singularities. *Soft Matter* **2018,** *14* (12), 2227-2233.

[34] Schutzius, T. M.; Graeber, G.; Elsharkawy, M.; Oreluk, J.; Megaridis, C. M., Morphing and vectoring impacting droplets by means of wettability-engineered surfaces. *Sci. Rep.* **2014,** *4*, 7029.

[35] Li, H.; Fang, W.; Li, Y.; Yang, Q.; Li, M.; Li, Q.; Feng, X. Q.; Song, Y., Spontaneous droplets gyrating via asymmetric self-splitting on heterogeneous surfaces. *Nat. Commun.* **2019,** *10* (1), 950.

[36] Zhao, Z. P.; Li, H. Z.; Hu, X. T.; Li, A.; Cai, Z. R.; Huang, Z. D.; Su, M.; Li, F. Y.; Li, M. Z.; Song, Y. L., Steerable Droplet Bouncing for Precise Materials Transportation. *Adv. Mater. Interfaces* **2019,** *6* (21), 1901033.

[37] Li, J.; Hou, Y.; Liu, Y.; Hao, C.; Li, M.; Chaudhury, M. K.; Yao, S.; Wang, Z., Directional transport of high-temperature Janus droplets mediated by structural topography. *Nat. Phys.* **2016,** *12* (6), 606-612.

[38] Chu, F.; Wu, X., Fabrication and condensation characteristics of metallic superhydrophobic surface with hierarchical micro-nano structures. *Appl. Surf. Sci.* **2016,** *371*, 322-328.

[39] Chu, F.; Wu, X.; Wang, L., Meltwater Evolution during Defrosting on Superhydrophobic Surfaces. *ACS Appl. Mater. Interfaces* **2018,** *10* (1), 1415-1421.

[40] Bartolo, D.; Josserand, C.; Bonn, D., Retraction dynamics of aqueous drops upon impact on non-wetting surfaces. *J. Fluid Mech.* **2005,** *545*,329-338.

[41] Eggers, J.; Fontelos, M. A.; Josserand, C.; Zaleski, S., Drop dynamics after impact on a solid wall: Theory and simulations. *Phys. Fluids* **2010,** *22* (6), 062101.

[42] Laan, N.; de Bruin, K. G.; Bartolo, D.; Josserand, C.; Bonn, D., Maximum Diameter of Impacting Liquid Droplets. *Phy. Rev. Appl.* **2014,** *2* (4),044018.

[43] Liu, X.; Zhang, X.; Min, J., Spreading of droplets impacting different wettable surfaces at a Weber number

close to zero. *Chem. Eng. Sci.* **2019,** *207*, 495-503.

[44] Qu, J.; Yang, Y.; Yang, S.; Hu, D.; Qiu, H., Droplet impingement on nano-textured superhydrophobic surface: Experimental and numerical study. *Appl. Surf. Sci.* **2019,** *491*, 160-170.

[45] Li, S.; Chu, F.; Zhang, J.; Brutin, D.; Wen, D., Droplet jumping induced by coalescence of a moving droplet and a static one: Effect of initial velocity. *Chem. Eng. Sci.* **2020,** *211*, 115252.

TABLE OF CONTENTS

Directional transportation of an impacting droplet